

Properties of the After Kernel

Philip M. Long
Google
plong@google.com

Abstract

The Neural Tangent Kernel (NTK) is the wide-network limit of a kernel defined using neural networks at initialization, whose embedding is the gradient of the output of the network with respect to its parameters. We study the “after kernel”, which is defined using the same embedding, except after training, for neural networks with standard architectures, on binary classification problems extracted from MNIST and CIFAR-10, trained using SGD in a standard way. For some dataset-architecture pairs, after a few epochs of neural network training, a hard-margin SVM using the network’s after kernel is much more accurate than when the network’s initial kernel is used. For networks with an architecture similar to VGG, the after kernel is more “global”, in the sense that it is less invariant to transformations of input images that disrupt the global structure of the image while leaving the local statistics largely intact. For fully connected networks, the after kernel is less global in this sense. The after kernel tends to be more invariant to small shifts, rotations and zooms; data augmentation does not improve these invariances. The (finite approximation to the) conjugate kernel, obtained using the last layer of hidden nodes, sometimes, but not always, provides a good approximation to the NTK and the after kernel.

Training a network with a larger learning rate (while holding the training error constant) produces a better kernel, as measured by the test error of a hard-margin SVM. The after kernels of networks trained with larger learning rates tend to be more global, and more invariant to small shifts, rotations and zooms.

1 Introduction

The neural tangent kernel (NTK) [27, 21, 14, 35, 34] has generated intense interest in recent years (see [21, 20, 10, 4, 62, 13, 31, 6, 11]). Its definition makes reference to a neural network at initialization. If θ_0 are the original parameters of the network, and f_{θ_0} is the function computed by the network then,

$$K_{\text{FNKT}}(x, x') = \phi(x) \cdot \phi(x'),$$

where $\phi(x)$ is the Jacobian of the function mapping θ to $f_{\theta}(x)$, evaluated at θ_0 . The NTK is a limit of K_{FNKT} (the “F” stands for “finite”) as the width of a network goes to infinity [57, 5]. Standard proofs using the NTK exploit the fact that, under conditions on the width, initialization, and learning rate, a first-order Taylor approximation of the objective function around the initial solution remains accurate throughout training. That is, the algorithm is learning a linear classifier over features that were determined at initialization.

A kernel analogous to the FNKT could also be defined after training. In this paper, we call this the *after kernel*. The after kernel was previously studied by Fort, et al [22], by evaluating

algorithms that replace the objective function of neural network training with its first-order Taylor expansion, after different amounts of training, effectively training a model using the after kernel. They showed that, after a few epochs of training, the after kernel is “better” than the NTK, and that additional epochs of training continue to improve it, but more gradually. Baratin, et al [8] showed experimentally that, for various architectures on CIFAR10 and MNIST, much of the energy of the spectrum of the after kernel is concentrated in a few eigenvalues, and that the alignment of the kernel with the labels increases.

In this paper, we further study the after kernel. We work with two binary classification problems defined using MNIST (3-vs-8 and 5-vs-6), and one using CIFAR10 (cats-vs-dogs). We use two architectures, one inspired by VGG [51], along with a depth-four, fully connected network. We chose VGG because it is relative simple and canonical, but includes several elements that are part of the standard practice of neural networks, including the use of convolutional layers, max pooling, and analysis of the image on multiple scales. We experimented with fully connected networks because they are, in a sense, the most basic and canonical neural networks, and, as such, are often the subject of theoretical analysis. We were especially interested in the extent to which phenomena observed in fully connected networks could also be found in convolutional networks. Many of our experiments with the VGG-like network use a network with approximately 100K parameters. We also experiment with a larger network, which we call the mega-VGG-like architecture, because it has roughly one million parameters. To obtain instances of the after kernel, we train neural networks with these architectures using Keras [15] with the default hyper-parameters. The details are in Section 2, and code is available online [37]. One noteworthy point is that all results were averaged over ten runs, where each run includes a random initialization of the network and random permutations of the training data.

We begin by conducting an experiment along the lines of [22], comparing the after kernel with the FNTK. To evaluate the quality of a kernel K , we evaluate the test-set error of the application of Algorithm 1 from [28] to compute the hard-margin SVM for K . Using the hard-margin SVM to evaluate the kernel is motivated in part by [39], who, building on the work of [53, 29, 30, 41, 55], showed that, under certain conditions, training neural networks to convergence produces a model equivalent to a hard-margin SVM applied with the after kernel. ([28] showed that their maximum margin algorithm converges much faster than SGD on the softmax loss, which was used to evaluate the kernel in the experiments in [22].) We show that, for fully connected networks on the MNIST problems, and VGG-like networks on the CIFAR10 cats-vs-dogs problem, the after kernel is much better than the FNTK in this sense.

Further, as seen in [22] under related conditions, we see that, even for the problems where the after kernel improves a lot on the FNTK, most of the improvement is seen after a few epochs. The test error of the SVM trained on the after kernel is, for quite a while, a lot better than the test error of the neural network. Consistent with the theory in [39], however, the neural network finally catches up. Informally, for much of training, for the most part, the deep-learning algorithm is effectively learning a linear model over features that were largely determined much earlier.

Next, we address the question of how “global” the kernels are. To measure this, following [42], we create artificial images in which the top left quadrant is swapped with the bottom right quadrant. Such swapping leaves local statistics largely intact, but disrupts the global structure of the image. To measure this invariance, we compute the average cosine similarity between embeddings computed using the unperturbed images with embeddings computed using the perturbed images. For the VGG-like networks, the after kernel is substantially more global than the FNTK. For fully

connected networks, however, this was not seen. The average similarity shot up after one epoch of training, after which it gradually decreased, settling down at a larger value than what was seen in the FNTK.

Next, we evaluate how invariant kernels are to slight perturbations of the images that should not affect their classifications. We evaluate three perturbations: shifts by one pixel, rotations by small angles, and slight zooms (obtained by cropping out a layer of pixels from the outside of the original image, and then resizing the cropped image to the original size). In most cases, the after kernel is more invariant to these perturbations.

The conjugate kernel [17] can be defined as the wide-network limit of a kernel whose embedding is obtained from a layered neural network by using the activations from the layer closest to the output layer. The components of the embedding of the conjugate kernel are also present in the FNTK. Accordingly, we will refer to an FNTK and its *conjugate projection*. The conjugate kernel was originally defined and analyzed using the network at initialization, but there is a natural counterpart after training, which we will call the conjugate projection of the after kernel. We evaluate the similarity between the FNTK and its conjugate projection using kernel alignment [16]. For VGG-like networks, the conjugate projection, whose embedding has many fewer features, and which is much easier to compute, provides a good approximation to the FNTK, and the after kernel is accurately approximated by its conjugate projection. For fully connected networks on the MNIST problems, however, the conjugate projection does not approximate the after kernel.

When its conjugate projection approximates the after kernel, as might be expected, the accuracy of SVM models using the respective kernels are similar. For VGG networks on the MNIST 5-vs-6 problem, however, the after kernel leads to better accuracy. On the CIFAR10 cats-vs-dogs data, where the after kernel and its conjugate projection are different, the after kernel leads to better accuracy for a while, but its conjugate projection catches up.

Next, we evaluate the effect of data augmentation on the learned kernel. We add two kinds of augmentation, random shifts and random rotations. Perhaps surprisingly, adding these augmentations tends not to improve the invariance of the after kernel to shifts, rotations and zooms, despite the fact that augmentations improve the test error, as seen in previous work.

In all of the above experiments, we used Keras’ default learning rate when training the networks. NTK proofs typically require a small learning rate, whereas models trained with a larger learning rate tend to generalize better [40, 52]. This is usually attributed to the tendency of training with a large learning rate to land in “wide minima”. However, the fact that small learning rates are required for staying in the NTK regime raises the question of whether another reason that large learning rates help is that they facilitate feature learning. Here, we evaluate this hypothesis using natural data with natural architectures. For each learning rate, we train a network until the training error reaches 0.01, and compare the after kernels. We find that the kernel of the networks trained with larger learning rates are better, in the sense that using them with SVM produces better test error. Kernels produced using the larger learning rates are also more global, as measured using invariance to swaps between the upper left and lower right quadrants. The large-learning rate kernels are also more invariant to small translations, rotations and zooms. Finally, while hard-margin classifiers trained with the after kernel are generally more accurate than when the conjugate kernel is used, the gap is smallest when the network is trained with a large learning rate. This is consistent with a view that higher learning rates lead to better high-level features, since, intuitively, the features at the output layer are the most high-level.

Additional related previous work. The most closely related previous work that we know of

was described above. Some recent papers have highlighted limitations of NTK analyses [55, 14, 59, 2, 36, 3, 18, 25]. A typical such theoretical result is a learning problem that can be solved (much) more efficiently using a neural network than by using kernel method with the NTK. Theoretical analyses with simple neural network architectures in idealized settings motivate research on natural data with practical architectures, identifying qualitative differences between the features used before and after training, demonstrating feature learning, and exploring its nature. A number of papers have described interesting properties of hidden units in a neural network, including how they change during training (see [50, 47, 48, 61, 26, 23, 60, 42, 43, 45]). Because, in a precise sense, the after kernel captures the features used by the network after training, its evolution during training is especially interesting. Lee, et al [33] compared learning with finite networks to application of the NTK and the conjugate kernel, which may be viewed as applying infinite networks. They also evaluated the effects of a number of modifications of the training process. Arora, et al [5] provided an algorithm to calculate the NTK for a convolutional neural network architecture, and compared the application of this kernel with the training of finite-width networks. (See also [44].) Yang and Hu [58] established conditions on the probability distributions used to sample the initial weights, and the step size of gradient descent, that imply that feature learning takes place, and conditions that imply that it does not. They also supported their theoretical analysis with experiments. Kornblith, et al [32] proposed using centered kernel alignment to measure the similarity of hidden nodes in the network; we use kernel alignment here to compare the neural tangent kernel and its conjugate projection.

Recent related work. After a preliminary version of this paper was published on ArXiv [38], [28] proposed new algorithms for finding the maximum margin linear separator – we use Algorithm 1 from their paper in this version. Recent papers evaluating the evolution of the after kernel include [49, 7].

2 Preliminaries and Methods

We focus on two-class classification.

If θ is the vector of initial weights for a neural network computing the function f_θ , then *the finite neural tangent kernel* K_{FNTK} is defined by $K_{\text{FNTK}}(u, v) = (\nabla_\theta f_\theta(u)) \cdot (\nabla_\theta f_\theta(v))$. The *after kernel* is defined the same way after training.

A *layered neural network* takes as input x , and transforms it using a processing layer g_1 , to produce a hidden layer $h_1(x) = g_1(x)$ of nodes, then applies another processing layer g_2 to h_1 , producing $h_2(x) = g_2(h_1(x))$, and so on. The final processing layer g_L , produces a scalar output $f(x) = g_L(h_{L-1}(x))$.

The *conjugate projection* K_c is defined by $K_c(u, v) = h_{L-1}(u) \cdot h_{L-1}(v)$.

Most of our experiments use networks with an architecture similar to VGG [51]. They are convolutional networks with two blocks of layers, followed by a fully connected layer. The first block consists of two convolutional layers with 26 channels each, 3×3 filters, and ReLU activations, followed by a max-pooling layer with stride 2 and pool size 2. The second block is similar, except with 52 channels. We call these networks VGG-like networks. (The number of channels was chosen so that the number of parameters of the network is approximately 100K, which is much more than the number of training examples. Additional experimental support for the proposition that the networks in this paper are sufficiently overparameterized may be found in Appendix A.)

We also experiment with larger networks where the number of channels in the convolutional

layers are 119 and 238 respectively. We refer to these as the *mega-VGG-like networks* because they have approximately one million parameters.

We also experiment with fully connected networks with four hidden layers of width 94. This was chosen so that the model has approximately 100K parameters.

Finally, for some unit tests, we experimented with a network that simply computes the sum of its inputs, and passes the result through fully connected layer with ReLU activations and width 16, followed by a fully connected layer with one output. While this network is not useful for classification, and, as such, is not a object of study itself, it is translation and rotation invariant, so it *is* useful for unit tests of the processes and code evaluating these invariances; we used it for this.

These networks were implemented using Tensorflow [1] and Keras [15]. In particular, for all the networks, all of the weights of all of the layers were initialized using the default initializer for Keras.

In most of our experiments, training was conducted without data augmentation. When data augmentation was used, it was implemented using the Keras ImageDataGenerator class, with a rotation range of 15 degrees, width shift range of 1, and height shift range of 1.

We trained the networks using the Keras implementation of SGD, with the default batch size and step size. We varied the number of epochs of training, using values 0, 1, 3, 10, 30, 100, and 200.

We trained linear models on features extracted from the neural networks. For this, we used Algorithm 1 from [28]. Prior to linear training, the extracted features were rescaled so that the average of the L_2 -norms of the features was one. (Note that, in principle, rescaling the features does not affect the output of the maximum margin algorithm. In practice, however, the rescaling was needed for numerical purposes.)

We experimented with three binary classification datasets: (a) the 3 and 8 classes from MNIST; (b) the 5 and 6 classes from MNIST, and (c) the cat and dog classes from CIFAR10.

To evaluate the quality of kernels, we trained hard-margin SVM classifiers on them and measured the test error. We used all of the training data, both to train the deep networks from which the kernels were extracted, and to train the SVM models using those kernels.

To evaluate the translation invariance of a kernel K for each image x in the test set, for the embedding ϕ associated with K , and for the images $s_h(x)$ and $s_v(x)$ obtained by shifting x one pixel to the right, and one pixel down, we computed the cosine similarity with $\phi(x)$ and $\phi(s_h(x))$, and the cosine similarity with $\phi(x)$ and $\phi(s_v(x))$. We then average all of these similarities.

We measured rotation invariance similarly to translation invariance, except rotating the images $1/4$ radians clockwise and counterclockwise, instead of shifting them.

We measured invariance to zooms as follows. For each image x , we obtained a perturbed image $z(x)$ cropping the outermost pixels from x , produced a cropped image $c(x)$ with height and width two less than x 's. We then resized $c(x)$ to the original size of x , producing $z(x)$, using TensorFlow's resize command, with the default parameters. We computed the cosine similarity between x and $z(x)$, and average the result over all of the examples in the test set.

We measured the extent to which a kernel is based on local properties of an image as follows. For each image x in the test set, we computed a perturbed image $s(x)$ by swapping the upper left quadrant of x with its lower right quadrant. We then computed the cosine similarity between the embeddings of x and $s(x)$ and averaged over all examples in the test set. Note that the local statistics of x and $s(x)$ are similar, but, especially in MNIST, swapping the upper right and lower left quadrants materially disrupts that global properties of the image.

We measured the kernel alignment [16, 32] between the NTK and its conjugate projection, both before and after training. To measure the alignment between two kernels, we computed Gram

matrices G and H for the respective kernels on the test data, and used $\frac{\text{vec}(G) \cdot \text{vec}(H)}{\sqrt{\text{vec}(G) \cdot \text{vec}(G)} \sqrt{\text{vec}(H) \cdot \text{vec}(H)}}$, where $\text{vec}(G)$ and $\text{vec}(H)$ are flattenings of G and H .

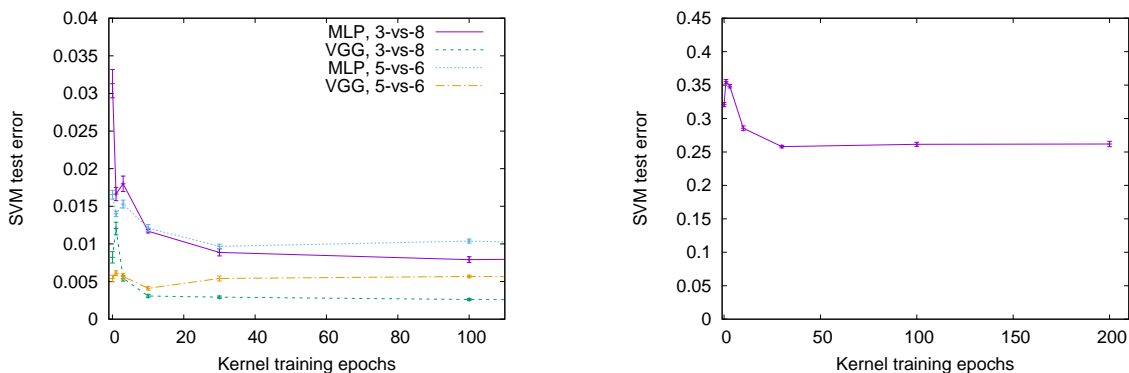
In addition to measuring the effect of the number of epochs of training of the neural network on properties of the after kernel, we also measured the effect of the learning rate used to train the neural network. In these experiments, the neural network was trained until the training loss was at most 0.01. For the MNIST data sets, we used learning rates 0.001, 0.003, 0.01, 0.03 and 0.1. For the CIFAR10 data set, we used learning rates 0.01, 0.02, 0.03, 0.04. For each learning rate, we evaluated the quality of the kernel, and its invariances, the same way as in the experiments that varied the number of epochs of neural network training.

Every experiment was repeated 10 times for different random initializations of the neural network weights, the results were averaged, and confidence intervals were computed.

3 Results

Figure 1 plots the test error of the hard margin SVM using the after kernel, as a function of the number of epochs that the network was trained before it was used to determine the kernel. The FNTK corresponds to zero epochs of training. When the kernel is computed using a fully connected network, the kernel quickly improves after a few epochs of training. For the VGG networks on the MNIST problems, the FNTK was already pretty good, though some improvement seems to be seen for the 3-vs-8 problem. For the VGG network on the CIFAR-10 problem, the after kernel is also much better than the FNTK.

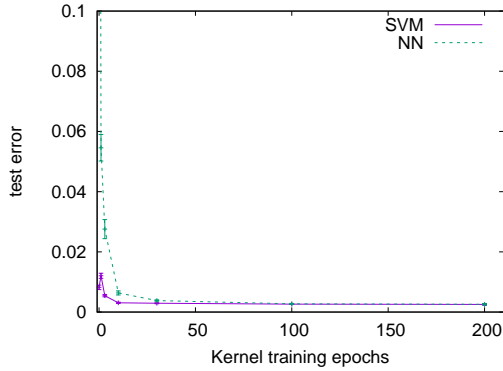
Figure 2 once again plots to test error of the hard-margin SVM with the after kernel, and also plots the test error of the network used to produce the kernel. Figure 3 provides the same plots, but concentrated on the portion of the curve regarding the early stage of training. The kernel is learned first, and then the network. Ultimately, the test error of the neural network catches up with the test error of the SVM trained with its after kernel, consistent with the theory in [39].



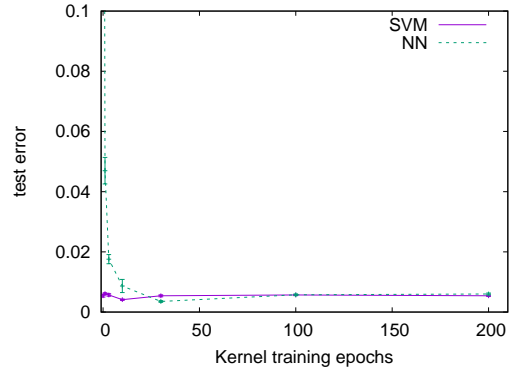
(a) The average test error of a hard margin SVM on MNIST, as a function of the number of epochs of training of the neural network used to produce the kernel. Results are plotted for fully connected networks, and VGG-like networks.

(b) The average test error of a hard margin SVM on a CIFAR-10 cats-vs-dogs binary classification problem, as a function of the number of epochs of training of the neural network used to produce the kernel, for the VGG-like network.

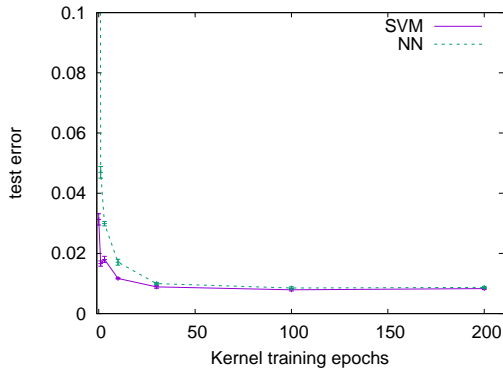
Figure 1



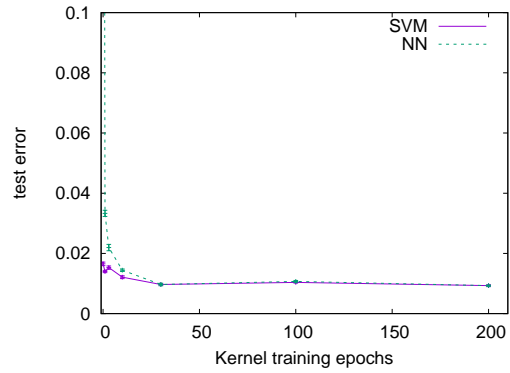
(a) The plot for the VGG-like network on MNIST 3-vs-8.



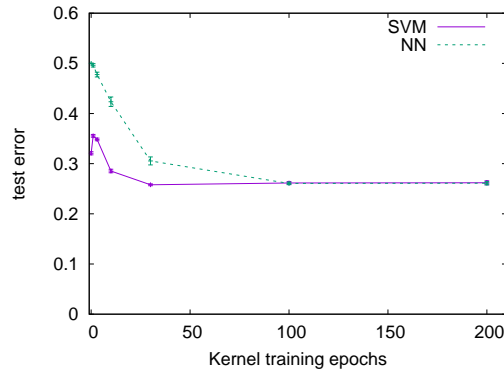
(b) The plot for the VGG-like network on MNIST 5-vs-6.



(c) The plot for the fully connected network on MNIST 3-vs-8.

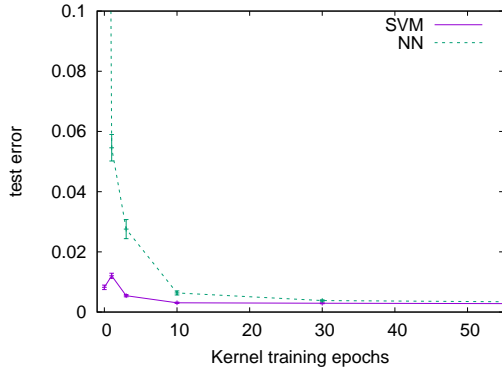


(d) The plot for the fully connected network on MNIST 5-vs-6.

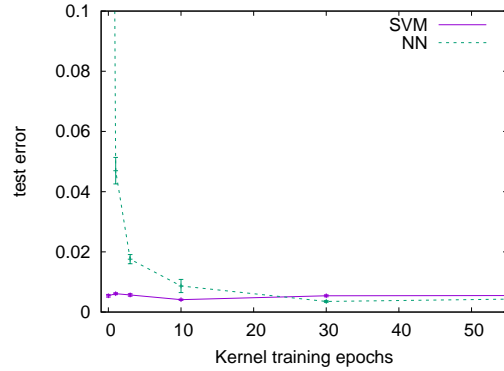


(e) The plot for the VGG-like network on CIFAR10 cats-vs-dogs.

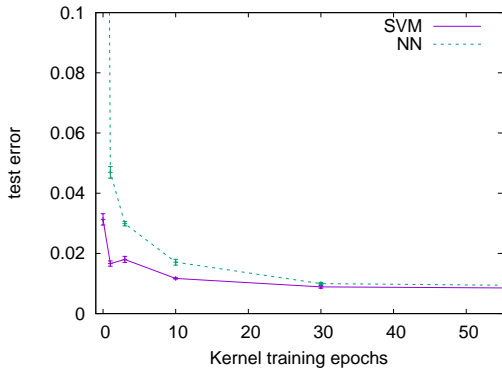
Figure 2: Plots of the average test error of a hard margin SVM, as a function of the number of epochs of training of the neural network used to produce the kernel, along with the test error of the neural network used to produce the kernel, for different architecture/dataset pairs.



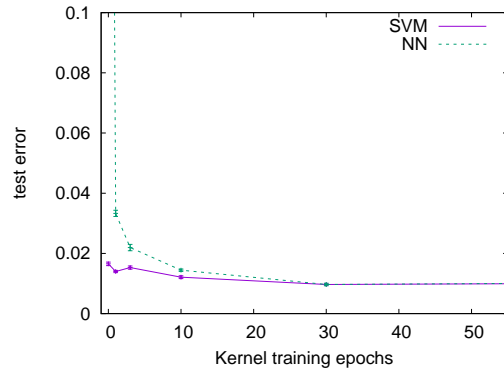
(a) The plot for the VGG-like network on MNIST 3-vs-8.



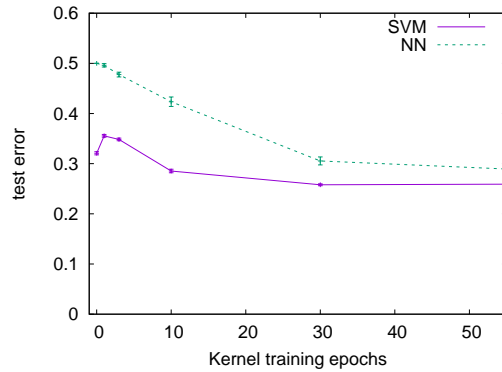
(b) The plot for the VGG-like network on MNIST 5-vs-6.



(c) The plot for the fully connected network on MNIST 3-vs-8.

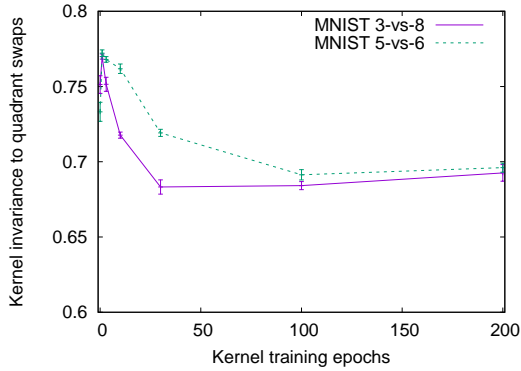


(d) The plot for the fully connected network on MNIST 5-vs-6.

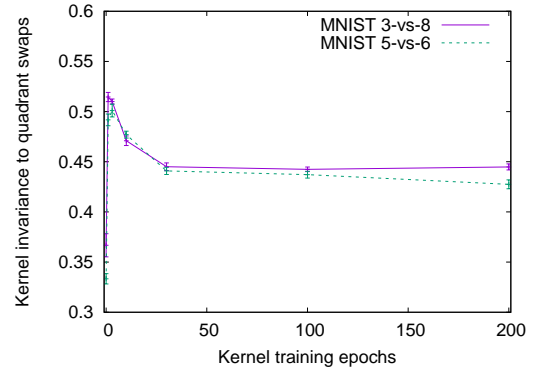


(e) The plot for the VGG-like network on CIFAR10 cats-vs-dogs.

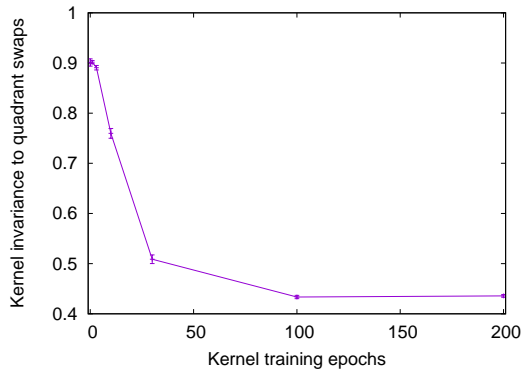
Figure 3: Plots of the average test error of a hard margin SVM, as a function of the number of epochs of training of the neural network used to produce the kernel, along with the test error of the neural network used to produce the kernel, for different architecture/dataset pairs.



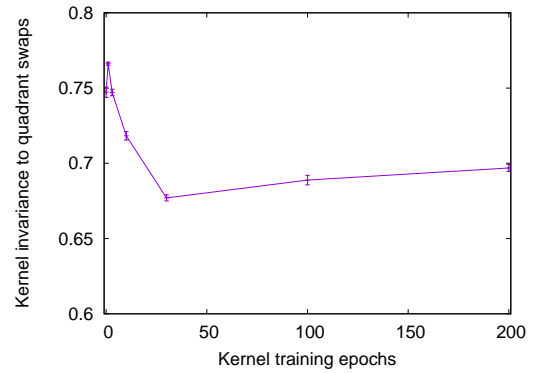
(a) The plot for VGG networks on two MNIST two-class problems.



(b) The plot for fully connected networks on two MNIST two-class problems.



(c) The plot for the VGG-like network on the CIFAR10 cats-vs-dogs problem.



(d) The plot for the mega-VGG-like network on the MNIST 3-vs-8 problem.

Figure 4: Plots of the average cosine similarity between features computed from the original image, and features computed from an image with two quadrants swapped, for the after kernel, as a function of the number of epochs of training of the neural network used to produce the kernel, for different architecture/dataset pairs.

Figure 4a plots the invariance of the features associated with the after kernel to swapping the top left quadrant and the bottom right quadrant, for test images. Recall that this is averaged over 10000 test examples and 10 training runs. These swaps largely preserve local statistics, so the reduction seen in Figure 4a in the insensitivity to these swaps is an indication that the kernel depends more on global properties of the image.

Figure 4b is the analogous plot for fully connected networks on the MNIST 3-vs-8 problem. The decreasing trend in swap-invariance with the number of rounds of training is consistent with the results for the VGG networks. However, the swap-invariance at initialization is less, and is the least ever seen. This could be because, for fully connected networks at initialization, many of the features are nonsense, informally, computing a function that is a locality sensitive hash of the input image. A non-local perturbation of the image then produces unrelated features. Overall, the curves are consistent with the possibility that, in fully connected networks, local features are learned first, then global features.

Figure 4c is the analogous plot for the VGG-like network on the CIFAR10 cats-vs-dogs problem. The swap-invariance decreases substantially, showing that the kernel depends more on global properties of the image. The effect may be greatest with the CIFAR10 because global information is needed to a greater extent to differentiate between the classes.

Figure 4d is the analogous plot for the mega-VGG-like network. For this bigger network, the after-kernel has significantly less swap invariance.

Figure 5 plots how invariant kernels are to different perturbations of the inputs, for different combinations of architectures, data sets, and number of rounds of training.

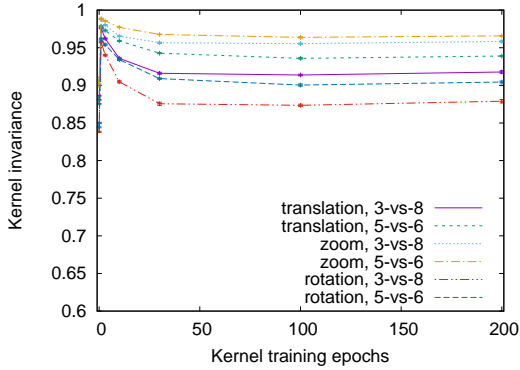
In all of the cases in the plot, the invariance shoots up after one epoch of training, then decreases as training continues. In most cases, the invariance settles down to a value larger than the FNTK. The fully connected network’s kernel starts out less invariant, and continues to be throughout training. The after kernel for the VGG-like network on CIFAR10 is much less rotation invariant than at initialization.

Figure 6a plots the alignments between the after kernel and its conjugate projection, for the VGG-like and mega-VGG-like networks, after different training times. The conjugate projection, which can be computed much more efficiently, remains a good approximation throughout, but is an especially good approximation at initialization. Figure 6b plots the alignments between the after kernel and its conjugate projection, for the fully connected networks, as a function of the number of epochs of training. The conjugate projection is a good approximation at initialization, but becomes much less so after training. Figure 6c plots the alignments between the after kernel and its conjugate projection, for the VGG-like network, as a function of the number of epochs of training. Here again, the conjugate projection is a good approximation at initialization, but becomes much less so after training.

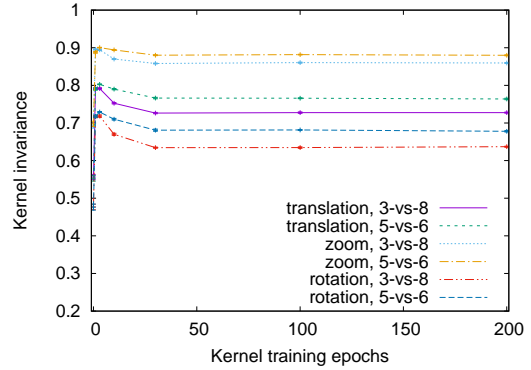
Figure 7 plots the test error of hard-margin SVM classifiers using the after kernel and its conjugate projection, as a function of the number of epochs used to train the kernels. In most cases, the classifier computed using the conjugate kernel is nearly as accurate as the classifier that uses the after kernel. It appears that the features closest to the output layer are the most useful. An exception, however, is the case of VGG networks on MNIST 5-vs-6, where the hard-margin classifier using the after kernel is substantially more accurate.

Figure 8 plots the invariances of the kernels to translations, zooms and rotations, when models are trained both with and without data augmentation.

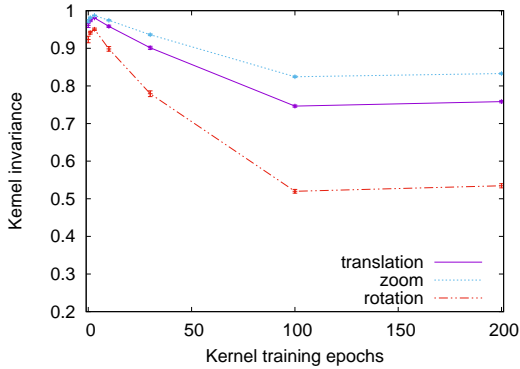
As a sanity check, Figure 16 in Appendix B reproduces the well-known fact that data augmenta-



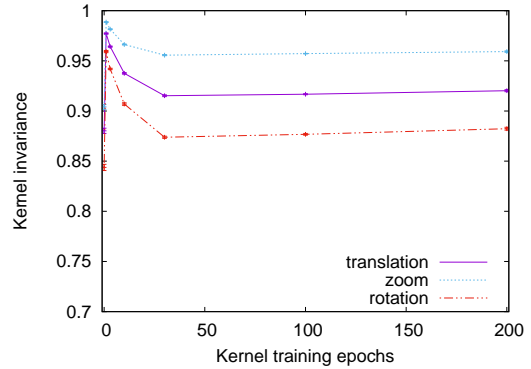
(a) The plot for VGG networks on two MNIST two-class problems.



(b) The plot for fully connected networks on two MNIST two-class problems.



(c) The plot for the VGG-like network on the CIFAR10 cats-vs-dogs problem.



(d) The plot for the mega-VGG-like network on the MNIST 3-vs-8 problem.

Figure 5: Plots of the average cosine similarity between features computed from the original image, and features computed from an image with various perturbations, for the after kernel, as a function of the number of epochs of training. The perturbations include shifts by one pixel, slight zooms, and rotations by small angles. The networks include the VGG-like network, the mega-VGG-like network, and the fully connected network. The datasets include MNIST 3-vs-8 and 5-vs-6 problems, and the CIFAR10 cats-vs-dogs problem.

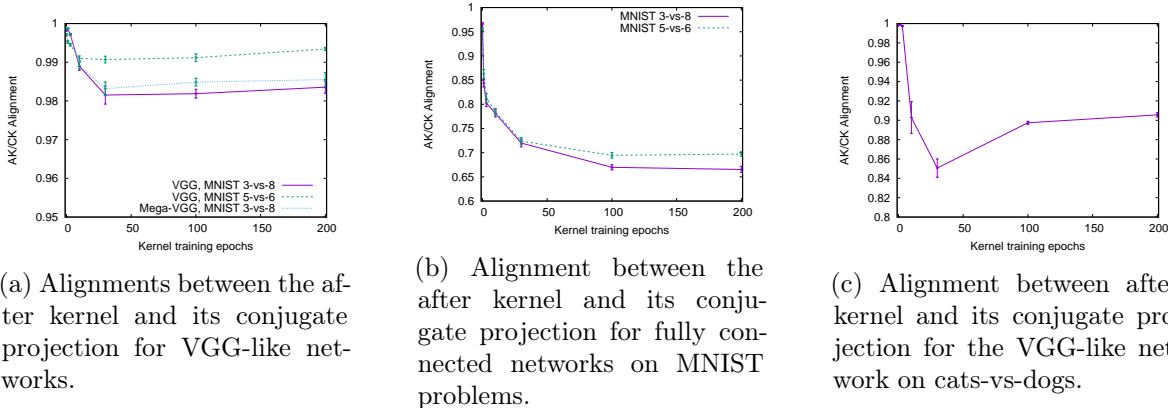


Figure 6: Alignments between the after kernel and the conjugate kernel.

tion improves the test accuracy of trained models, and that this carries over to the models trained with SVM using kernels trained with data augmentation.

Figure 9 plots the accuracy of the maximum margin classifier using the after kernel, along with the accuracy of the neural network used to produce the kernel, as a function of the learning rate. There is a general trend that a higher learning rate produces a better kernel, if the training error is held constant. On MNIST 3-vs-8, the maximum margin classifier had better test error than the neural network, despite the fact that the neural network was trained to almost zero error. Clearly, here, the neural network is not approximating the maximum margin with respect to the after kernel.

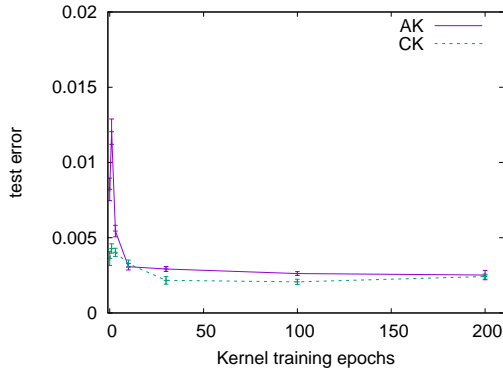
Figure 10 plots the swap invariance as a function of the learning rate. The features obtained with a large learning rate reflect global properties of the image to a greater extent.

Figure 11 plots the translation, room and rotation invariances as a function of the learning rate. Features obtained for larger learning rates are less invariant to these slight transformations of the image.

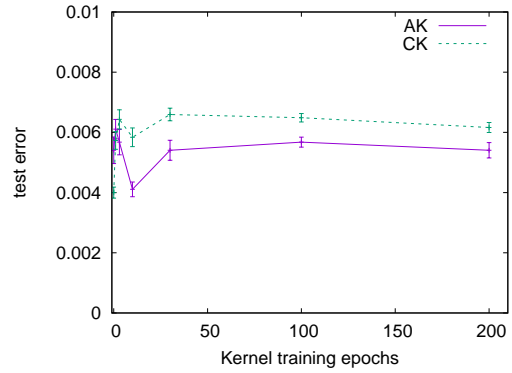
Figure 12 plots the alignment between the after kernel and the conjugate kernel, as a function of the learning rate. For VGG networks, the alignment is highest at the lowest learning rates, while the opposite holds for fully connected networks.

Figure 13 plots the test error of maximum margin classifiers using the after and the conjugate kernel. Generally, the after kernel provides better accuracy, though the conjugate kernel is more competitive overall at higher learning rates – this is consistent with a view that higher learning rates lead to better high-level features, since, intuitively, the features at the output layer are the most high-level.

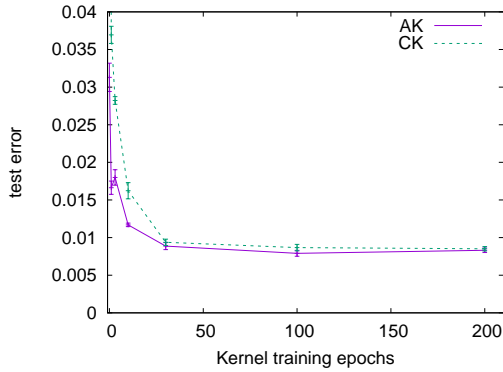
Figure 14 plots the translation, room and rotation invariances as a function of the learning rate, for data with augmentations. The trend that a higher learning rate leads to less invariance to these perturbations persists when augmentations are added, and is even greater in the case of CIFAR10.



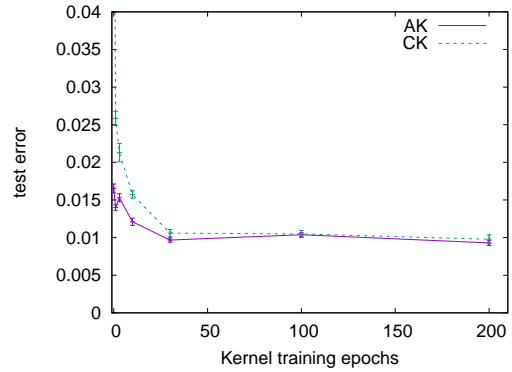
(a) The plot for VGG-like networks on MNIST 3-vs-8.



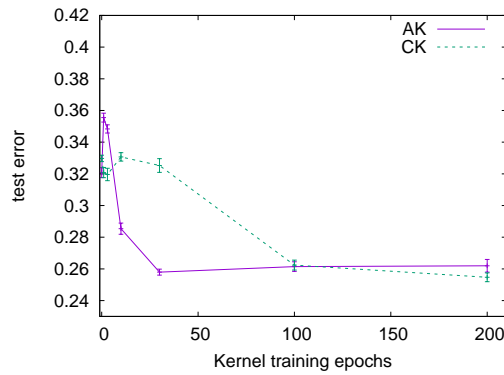
(b) The plot for VGG-like networks on MNIST 5-vs-6.



(c) The plot for fully connected networks on MNIST 3-vs-8.

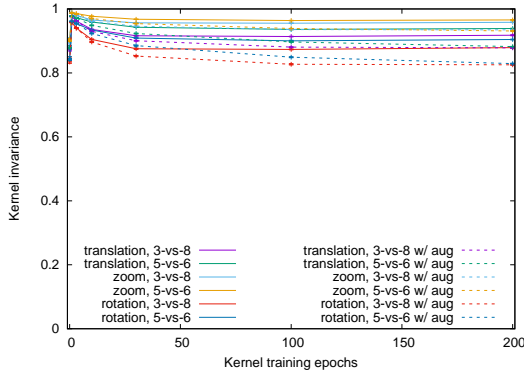


(d) The plot for fully connected networks on MNIST 5-vs-6.

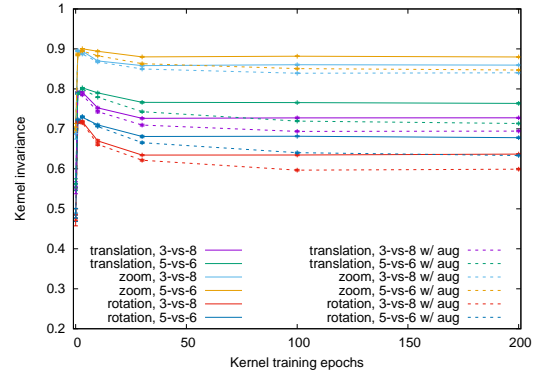


(e) The plot for the VGG-like network on cats-vs-dogs.

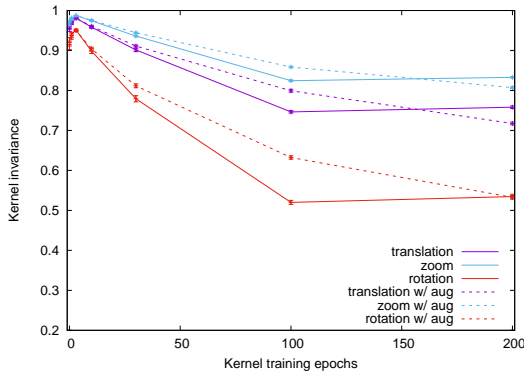
Figure 7: Test error of SVMs trained with the after kernel and the conjugate kernel for various architecture-dataset pairs.



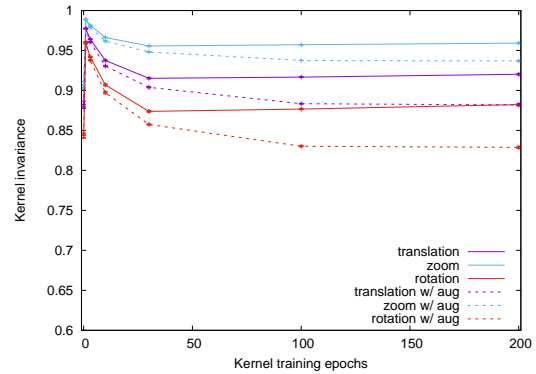
(a) The plot for VGG networks on two MNIST two-class problems.



(b) The plot for fully connected networks on two MNIST two-class problems.

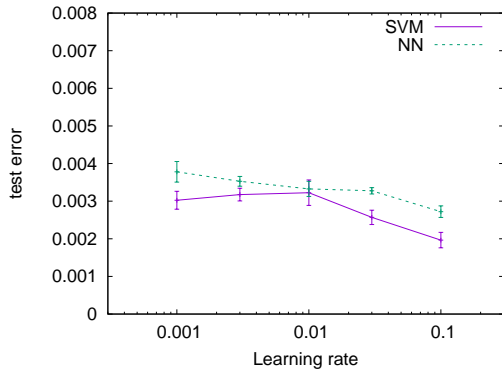


(c) The plot for the VGG-like network on the CIFAR10 cats-vs-dogs problem.

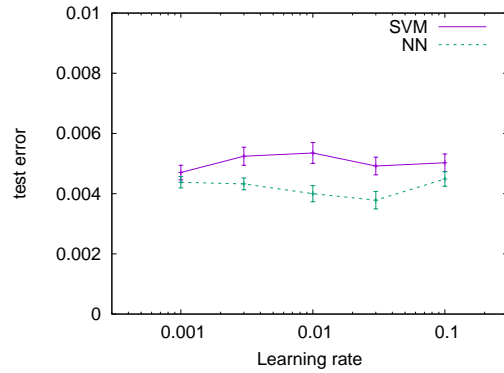


(d) The plot for the mega-VGG-like network on the MNIST 3-vs-8 problem.

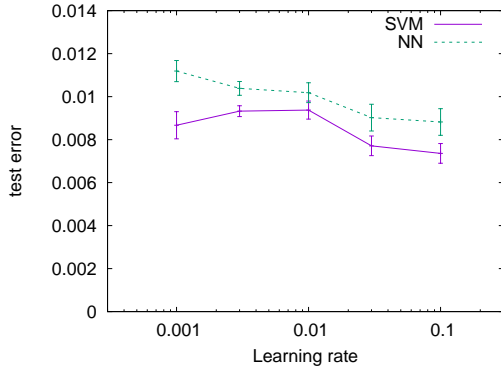
Figure 8: Plots of three invariances of kernels with and without data augmentation, as a function of the number of epochs of training.



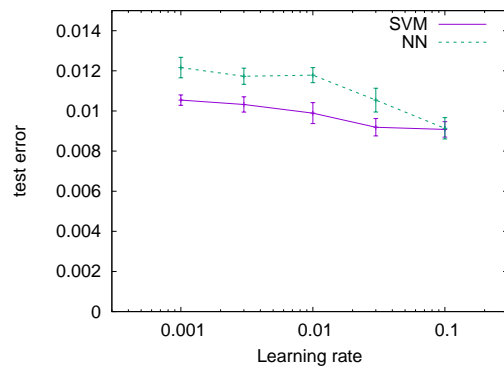
(a) The plot for the VGG-like network on MNIST 3-vs-8.



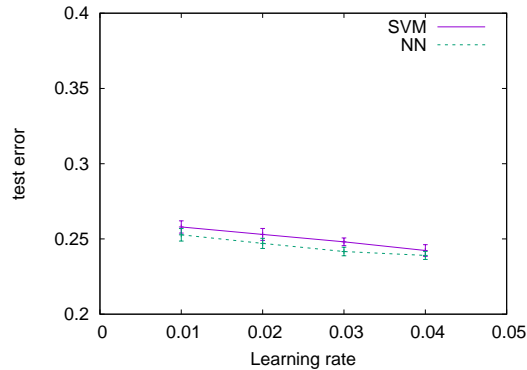
(b) The plot for the VGG-like network on MNIST 5-vs-6.



(c) The plot for the fully connected network on MNIST 3-vs-8.

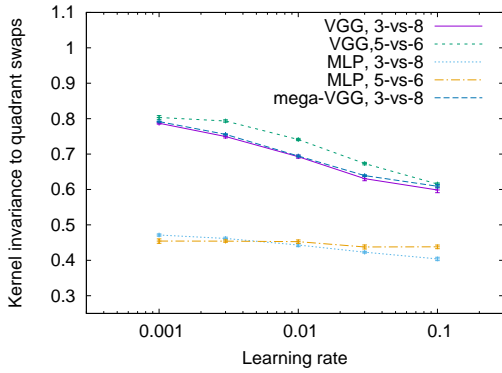


(d) The plot for the fully connected network on MNIST 5-vs-6.

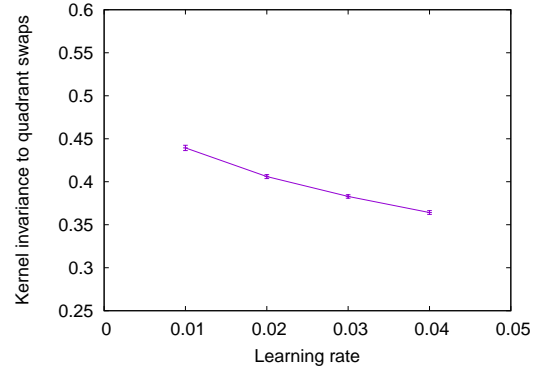


(e) The plot for the VGG-like network on CIFAR10 cats-vs-dogs.

Figure 9: Plots of the average test error of a hard margin SVM, as a function of the learning rate when the neural network used to produce the kernel, along with the test error of the neural network used to produce the kernel, for different architecture/dataset pairs.

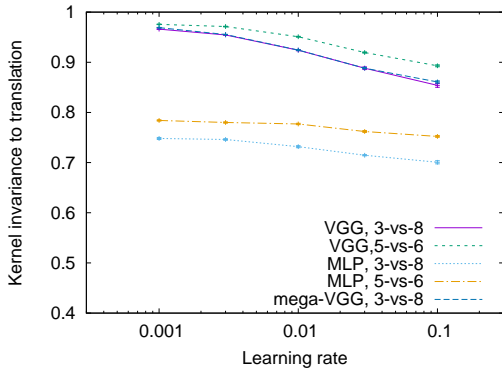


(a) The plot for MNIST two-class problems.

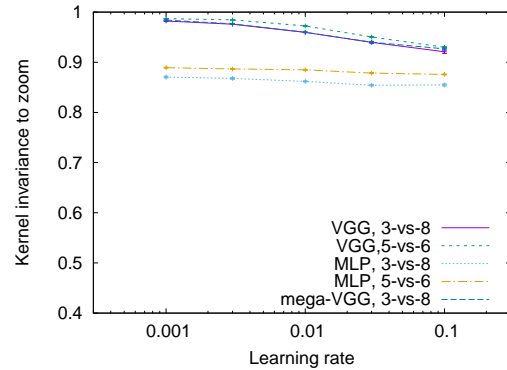


(b) The plot for VGG networks on CIFAR10 cats-vs-dogs.

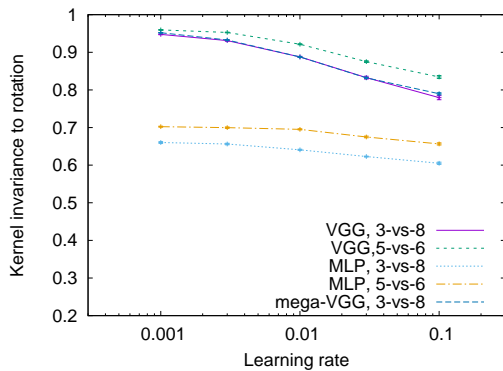
Figure 10: Plots of the average cosine similarity between features computed from the original image, and features computed from an image with two quadrants swapped, for the after kernel, as a function of learning rate, for different architecture/dataset pairs.



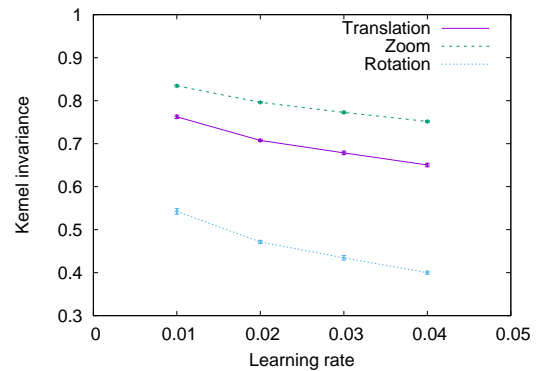
(a) The plot for translation invariance for MNIST two-class problems.



(b) The plot for zoom invariance for MNIST two-class problems.

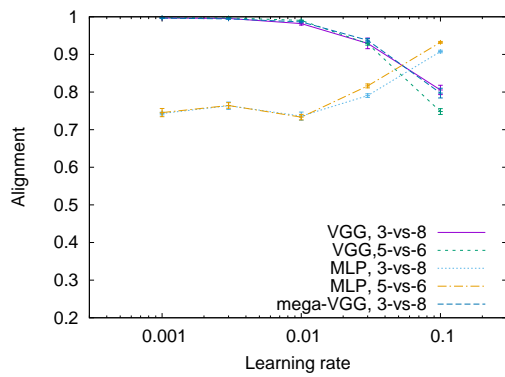


(c) The plot for rotation invariance for MNIST two-class problems.

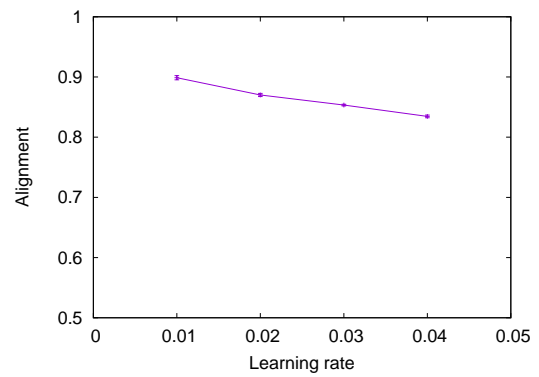


(d) The plot for VGG networks on CIFAR10 cats-vs-dogs.

Figure 11: Plots of translation, zoom, and rotation invariance, as a function of learning rate, for different architecture/dataset pairs.

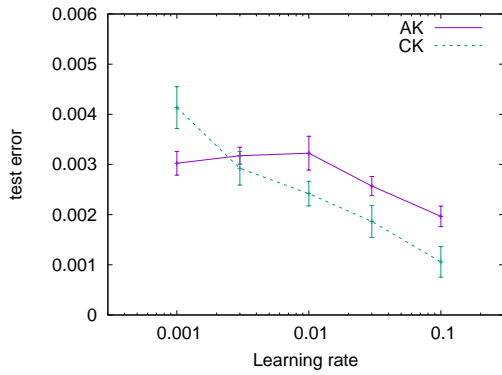


(a) The plot for MNIST problems.

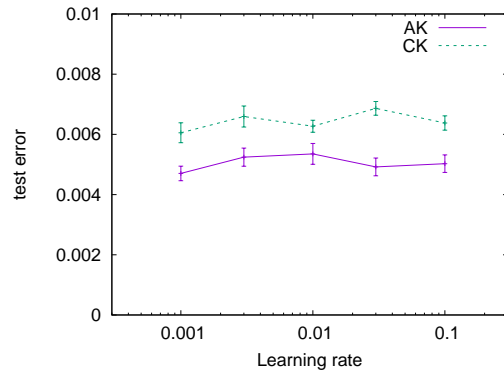


(b) The plot for CIFAR10 cats-vs-dogs.

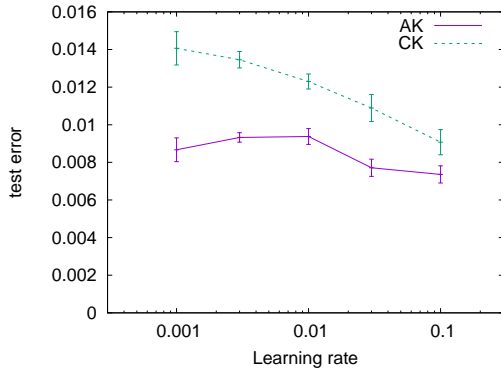
Figure 12: Alignments between the after kernel and the conjugate kernel.



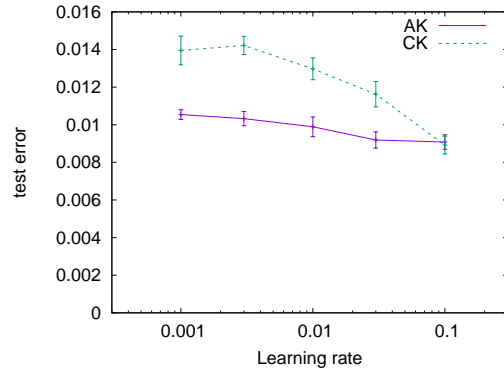
(a) The plot for VGG-like networks on MNIST 3-vs-8.



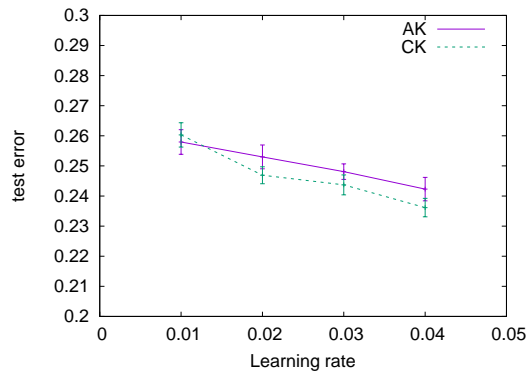
(b) The plot for VGG-like networks on MNIST 5-vs-6.



(c) The plot for fully connected networks on MNIST 3-vs-8.

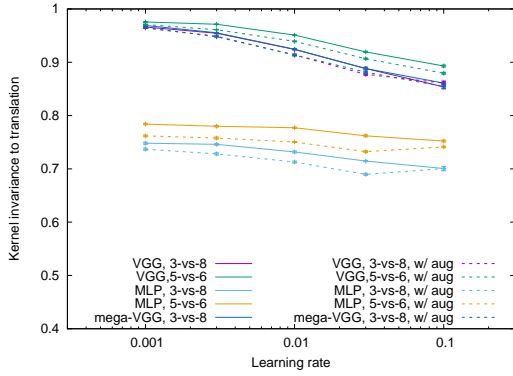


(d) The plot for fully connected networks on MNIST 5-vs-6.

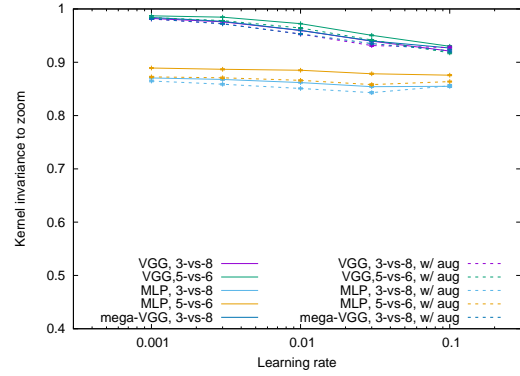


(e) The plot VGG-like networks on CIFAR10 cats-vs-dogs.

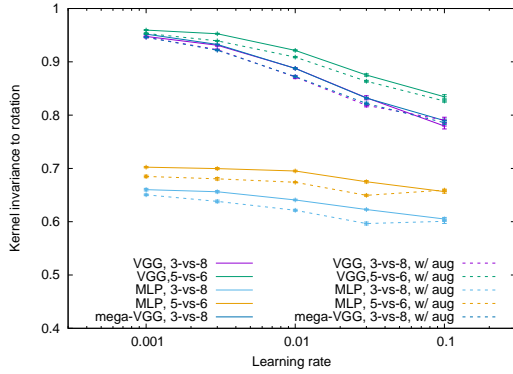
Figure 13: Test error of SVMs trained with the after kernel and the conjugate kernel, as a function of learning rate.



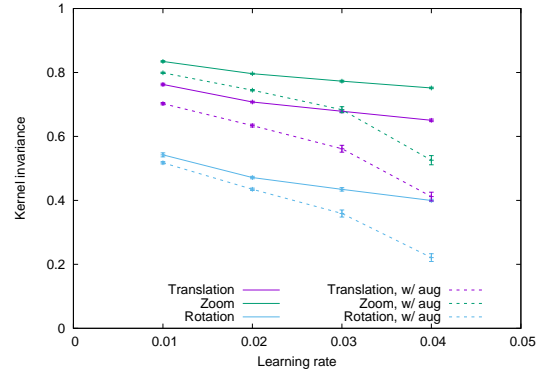
(a) Translation invariance for MNIST two-class problems.



(b) Zoom invariance for MNIST two-class problems.



(c) Rotation invariance for MNIST two-class problems.



(d) The plot for VGG networks on CIFAR10 cats-vs-dogs.

Figure 14: Plots of translation, zoom, and rotation invariance, as a function of learning rate, for different architecture/dataset pairs, for data with and without augmentations.

4 Discussion

When standard neural networks are trained in a standard way, the after kernel is often qualitatively quite different from the (finite) neural tangent kernel. The quality of the after kernel improves rapidly; it appears that the kernel is learned first, then the kernel classifier. Training a network with a larger learning rate produces a better kernel, even when the training error is held constant. The advantage of the kernel obtained with a larger learning rate can be seen both in the accuracy of an SVM trained with the kernel, and in invariance properties that meaningful features should be expected to have.

The kernel used with the network after training is not strongly invariant to small perturbations of the inputs. We were surprised that, in many cases, the degree of invariance degrades slowly in the later stages of training. Explaining this is a challenge for theory. Data augmentation did not make the after kernel more invariant to small perturbations.

Many additional questions could be addressed by modifying the code used in this research, which, as mentioned earlier, is available online [37]. For example, it would be interesting to evaluate the effect of contrastive training [12] on the evolution of the after kernel, in particular, on its invariances. Comparing properties of the after kernel for networks trained with EfficientNet [54] with networks trained with VGG could enhance understanding of why EfficientNet models are more accurate. Similarly, recent encouraging results with Visual Transformers [46, 9, 19] motivate study of the after kernel of these models. Examining the effect of the depth of the network is another obvious future direction. Comparing the dynamics when models are trained for NLP tasks with the dynamics arising from image data would be another interesting subject for study. Last, but not least, results on the effect of the scale of the initialization on the implicit bias of gradient descent in idealized theoretical settings [24, 56] motivate investigation of this effect on practical networks with real data; the code accompanying this paper [37] could be a useful tool for this.

Acknowledgements

We are grateful to Yamini Bansal, Peter Bartlett, Olivier Bousquet, Yuan Cao, Niladri Chatterji, Quanquan Gu, Ziwei Ji, Praneeth Netrapalli, Behnam Neyshabur, Hanie Sedghi, and Jascha Sohl-Dickstein valuable conversations. We also thank Ziwei Ji for code for Algorithm 1 from [28].

References

- [1] Martín Abadi, Ashish Agarwal, Paul Barham, Eugene Brevdo, Zhifeng Chen, Craig Citro, Greg S. Corrado, Andy Davis, Jeffrey Dean, Matthieu Devin, Sanjay Ghemawat, Ian Goodfellow, Andrew Harp, Geoffrey Irving, Michael Isard, Yangqing Jia, Rafal Jozefowicz, Lukasz Kaiser, Manjunath Kudlur, Josh Levenberg, Dandelion Mané, Rajat Monga, Sherry Moore, Derek Murray, Chris Olah, Mike Schuster, Jonathon Shlens, Benoit Steiner, Ilya Sutskever, Kunal Talwar, Paul Tucker, Vincent Vanhoucke, Vijay Vasudevan, Fernanda Viégas, Oriol Vinyals, Pete Warden, Martin Wattenberg, Martin Wicke, Yuan Yu, and Xiaoqiang Zheng. TensorFlow: Large-scale machine learning on heterogeneous systems, 2015. Software available from tensorflow.org.

- [2] Zeyuan Allen-Zhu and Yuanzhi Li. What can ResNet learn efficiently, going beyond kernels? In *NeurIPS*, pages 9015–9025, 2019.
- [3] Zeyuan Allen-Zhu and Yuanzhi Li. Backward feature correction: How deep learning performs deep learning. *CoRR*, abs/2001.04413, 2020.
- [4] Zeyuan Allen-Zhu, Yuanzhi Li, and Zhao Song. A convergence theory for deep learning via over-parameterization. In *ICML*, pages 242–252, 2019.
- [5] Sanjeev Arora, Simon S. Du, Wei Hu, Zhiyuan Li, Ruslan Salakhutdinov, and Ruosong Wang. On exact computation with an infinitely wide neural net. In *NeurIPS*, pages 8139–8148, 2019.
- [6] Sanjeev Arora, Simon S. Du, Wei Hu, Zhiyuan Li, and Ruosong Wang. Fine-grained analysis of optimization and generalization for overparameterized two-layer neural networks. In *ICML*, pages 322–332, 2019.
- [7] Alexander Atanasov, Blake Bordelon, and Cengiz Pehlevan. Neural networks as kernel learners: The silent alignment effect. *arXiv preprint arXiv:2111.00034*, 2021.
- [8] Aristide Baratin, Thomas George, César Laurent, R Devon Hjelm, Guillaume Lajoie, Pascal Vincent, and Simon Lacoste-Julien. Implicit regularization via neural feature alignment. In *International Conference on Artificial Intelligence and Statistics*, pages 2269–2277, 2021.
- [9] Irwan Bello, Barret Zoph, Ashish Vaswani, Jonathon Shlens, and Quoc V Le. Attention augmented convolutional networks. In *Proceedings of the IEEE/CVF international conference on computer vision*, pages 3286–3295, 2019.
- [10] Yuan Cao and Quanquan Gu. Generalization bounds of stochastic gradient descent for wide and deep neural networks. In *NeurIPS*, pages 10835–10845, 2019.
- [11] N. Chatterji, P. M. Long, and P. L. Bartlett. When does gradient descent with logistic loss interpolate using deep networks with smoothed relu activations? *COLT*, 2021.
- [12] Ting Chen, Simon Kornblith, Mohammad Norouzi, and Geoffrey Hinton. A simple framework for contrastive learning of visual representations. In *International conference on machine learning*, pages 1597–1607, 2020.
- [13] Zixiang Chen, Yuan Cao, Difan Zou, and Quanquan Gu. How much over-parameterization is sufficient to learn deep relu networks? *ICLR*, 2021.
- [14] Lénaïc Chizat, Edouard Oyallon, and Francis R. Bach. On lazy training in differentiable programming. In *NeurIPS*, pages 2933–2943, 2019.
- [15] François Chollet. Keras, 2015.
- [16] Nello Cristianini, John Shawe-Taylor, André Elisseeff, and Jaz Kandola. On kernel-target alignment. In *Advances in Neural Information Processing Systems*, 2002.
- [17] Amit Daniely, Roy Frostig, and Yoram Singer. Toward deeper understanding of neural networks: The power of initialization and a dual view on expressivity. In *NeurIPS*, pages 2253–2261, 2016.

- [18] Amit Daniely and Eran Malach. Learning parities with neural networks. In *NeurIPS*, 2020.
- [19] Alexey Dosovitskiy, Lucas Beyer, Alexander Kolesnikov, Dirk Weissenborn, Xiaohua Zhai, Thomas Unterthiner, Mostafa Dehghani, Matthias Minderer, Georg Heigold, Sylvain Gelly, Jakob Uszkoreit, and Neil Houlsby. An image is worth 16x16 words: Transformers for image recognition at scale. In *ICLR*, 2021.
- [20] Simon Du, Jason Lee, Haochuan Li, Liwei Wang, and Xiyu Zhai. Gradient descent finds global minima of deep neural networks. In *International Conference on Machine Learning*, pages 1675–1685, 2019.
- [21] Simon S. Du, Xiyu Zhai, Barnabás Póczos, and Aarti Singh. Gradient descent provably optimizes over-parameterized neural networks. In *ICLR*, 2019.
- [22] Stanislav Fort, Gintare Karolina Dziugaite, Mansheej Paul, Sepideh Kharaghani, Daniel M. Roy, and Surya Ganguli. Deep learning versus kernel learning: an empirical study of loss landscape geometry and the time evolution of the neural tangent kernel. In *NeurIPS*, 2020.
- [23] Jonathan Frankle and Michael Carbin. The lottery ticket hypothesis: Finding sparse, trainable neural networks. In *ICLR*, 2019.
- [24] Mario Geiger, Stefano Spigler, Arthur Jacot, and Matthieu Wyart. Disentangling feature and lazy training in deep neural networks. *Journal of Statistical Mechanics: Theory and Experiment*, 2020(11):113301, 2020.
- [25] Behrooz Ghorbani, Song Mei, Theodor Misiakiewicz, and Andrea Montanari. When do neural networks outperform kernel methods? In *NeurIPS*, 2020.
- [26] Aditya Golatkar, Alessandro Achille, and Stefano Soatto. Time matters in regularizing deep networks: Weight decay and data augmentation affect early learning dynamics, matter little near convergence. In *NeurIPS*, pages 10677–10687, 2019.
- [27] Arthur Jacot, Clément Hongler, and Franck Gabriel. Neural tangent kernel: Convergence and generalization in neural networks. In *NeurIPS*, pages 8580–8589, 2018.
- [28] Ziwei Ji, Nathan Srebro, and Matus Telgarsky. Fast margin maximization via dual acceleration. In *International Conference on Machine Learning*, pages 4860–4869, 2021.
- [29] Ziwei Ji and Matus Telgarsky. Gradient descent aligns the layers of deep linear networks. *arXiv preprint arXiv:1810.02032*, 2018.
- [30] Ziwei Ji and Matus Telgarsky. The implicit bias of gradient descent on nonseparable data. In *COLT*, 2019.
- [31] Ziwei Ji and Matus Telgarsky. Polylogarithmic width suffices for gradient descent to achieve arbitrarily small test error with shallow relu networks. In *ICLR*, 2020.
- [32] Simon Kornblith, Mohammad Norouzi, Honglak Lee, and Geoffrey E. Hinton. Similarity of neural network representations revisited. In *ICML*, 2019.

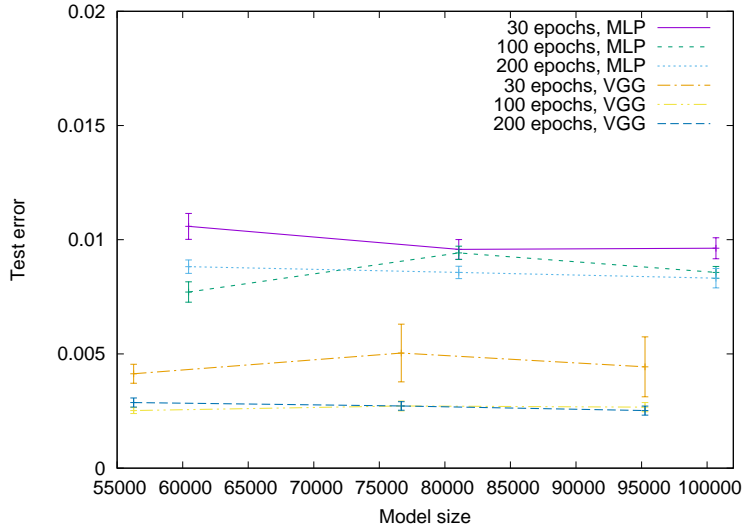
- [33] Jaehoon Lee, Samuel S. Schoenholz, Jeffrey Pennington, Ben Adlam, Lechao Xiao, Roman Novak, and Jascha Sohl-Dickstein. Finite versus infinite neural networks: an empirical study. In *NeurIPS*, 2020.
- [34] Jaehoon Lee, Lechao Xiao, Samuel S. Schoenholz, Yasaman Bahri, Roman Novak, Jascha Sohl-Dickstein, and Jeffrey Pennington. Wide neural networks of any depth evolve as linear models under gradient descent. In *NeurIPS*, pages 8570–8581, 2019.
- [35] Yuanzhi Li and Yingyu Liang. Learning overparameterized neural networks via stochastic gradient descent on structured data. In *NeurIPS*, pages 8168–8177, 2018.
- [36] Yuanzhi Li, Tengyu Ma, and Hongyang R. Zhang. Learning over-parametrized two-layer neural networks beyond NTK. In *COLT*, pages 2613–2682, 2020.
- [37] P. M. Long, 2021. https://github.com/google-research/google-research/tree/master/after_kernel.
- [38] Philip M Long. Properties of the after kernel. *arXiv preprint arXiv:2105.10585*, 2021. Version 1.
- [39] Kaifeng Lyu and Jian Li. Gradient descent maximizes the margin of homogeneous neural networks. *ICLR*, 2020.
- [40] Stephan Mandt, Matthew D Hoffman, and David M Blei. Stochastic gradient descent as approximate bayesian inference. *arXiv preprint arXiv:1704.04289*, 2017.
- [41] Mor Shpigel Nacson, Suriya Gunasekar, Jason D. Lee, Nathan Srebro, and Daniel Soudry. Lexicographic and depth-sensitive margins in homogeneous and non-homogeneous deep models. In *ICML*, pages 4683–4692, 2019.
- [42] Behnam Neyshabur, Hanie Sedghi, and Chiyuan Zhang. What is being transferred in transfer learning? In *NeurIPS*, 2020.
- [43] Thao Nguyen, Maithra Raghu, and Simon Kornblith. Do wide and deep networks learn the same things? uncovering how neural network representations vary with width and depth. In *International Conference on Learning Representations*, 2021.
- [44] Roman Novak, Lechao Xiao, Jiri Hron, Jaehoon Lee, Alexander A. Alemi, Jascha Sohl-Dickstein, and Samuel S. Schoenholz. Neural tangents: Fast and easy infinite neural networks in python. In *ICLR*, 2020.
- [45] Vardan Papyan, XY Han, and David L Donoho. Prevalence of neural collapse during the terminal phase of deep learning training. *Proceedings of the National Academy of Sciences*, 117(40):24652–24663, 2020.
- [46] Niki Parmar, Ashish Vaswani, Jakob Uszkoreit, Lukasz Kaiser, Noam Shazeer, Alexander Ku, and Dustin Tran. Image transformer. In *International Conference on Machine Learning*, pages 4055–4064, 2018.
- [47] Maithra Raghu, Justin Gilmer, Jason Yosinski, and Jascha Sohl-Dickstein. SVCCA: singular vector canonical correlation analysis for deep learning dynamics and interpretability. In *Advances in Neural Information Processing Systems*, pages 6076–6085, 2017.

- [48] Andrew M Saxe, Yamini Bansal, Joel Dapello, Madhu Advani, Artemy Kolchinsky, Brendan D Tracey, and David D Cox. On the information bottleneck theory of deep learning. *Journal of Statistical Mechanics: Theory and Experiment*, 2019(12):124020, 2019.
- [49] Haozhe Shan and Blake Bordelon. Rapid feature evolution accelerates learning in neural networks. *arXiv preprint arXiv:2105.14301*, 2021.
- [50] Ravid Shwartz-Ziv and Naftali Tishby. Opening the black box of deep neural networks via information. *CoRR*, 2017.
- [51] K. Simonyan and A. Zisserman. Very deep convolutional networks for large-scale image recognition. *ICLR*, 2015.
- [52] Samuel L. Smith and Quoc V. Le. A bayesian perspective on generalization and stochastic gradient descent. In *ICLR*, 2018.
- [53] Daniel Soudry, Elad Hoffer, Mor Shpigel Nacson, and Nathan Srebro. The implicit bias of gradient descent on separable data. In *ICLR*, 2018.
- [54] Mingxing Tan and Quoc Le. Efficientnet: Rethinking model scaling for convolutional neural networks. In *International Conference on Machine Learning*, pages 6105–6114, 2019.
- [55] Colin Wei, Jason D. Lee, Qiang Liu, and Tengyu Ma. Regularization matters: Generalization and optimization of neural nets v.s. their induced kernel. In *NeurIPS*, pages 9709–9721, 2019.
- [56] Blake E. Woodworth, Suriya Gunasekar, Jason D. Lee, Edward Moroshko, Pedro Savarese, Itay Golan, Daniel Soudry, and Nathan Srebro. Kernel and rich regimes in overparametrized models. In *COLT*, 2020.
- [57] Greg Yang. Scaling limits of wide neural networks with weight sharing: Gaussian process behavior, gradient independence, and neural tangent kernel derivation. *arXiv preprint arXiv:1902.04760*, 2019.
- [58] Greg Yang and Edward J Hu. Feature learning in infinite-width neural networks. *arXiv preprint arXiv:2011.14522*, 2020.
- [59] Gilad Yehudai and Ohad Shamir. On the power and limitations of random features for understanding neural networks. In *NeurIPS*, pages 6594–6604, 2019.
- [60] Chiyuan Zhang, Samy Bengio, Moritz Hardt, Michael C. Mozer, and Yoram Singer. Identity crisis: Memorization and generalization under extreme overparameterization. In *ICLR*, 2020.
- [61] Chiyuan Zhang, Samy Bengio, and Yoram Singer. Are all layers created equal? *arXiv preprint arXiv:1902.01996*, 2019.
- [62] Difan Zou and Quanquan Gu. An improved analysis of training over-parameterized deep neural networks. In *NeurIPS*, pages 2053–2062, 2019.

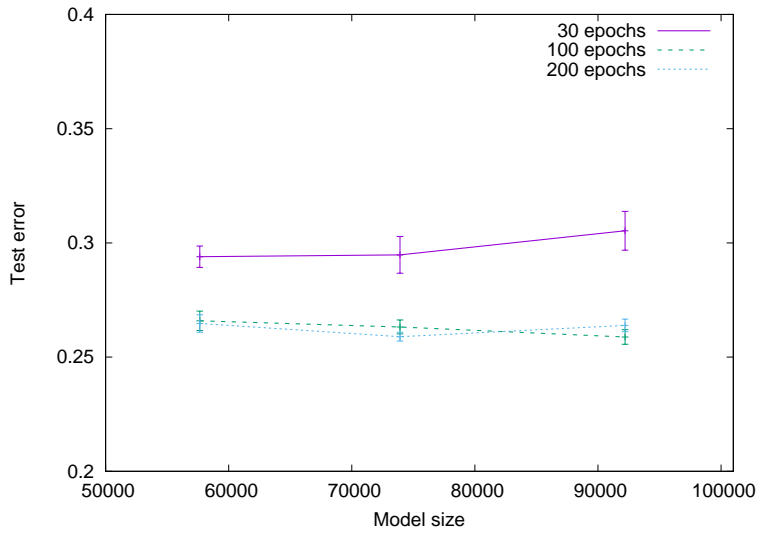
A The networks are sufficiently overparameterized

In this appendix, we describe experiments aimed at supporting the proposition that the networks in our study of the after kernel are sufficiently overparameterized. We varied the width of the networks, while otherwise holding the architecture fixed, as described in Section 2. In the case of the VGG-like networks, this was done by scaling down the number of channels in each convolutional layer, and, in the fully connected networks, this was done by reducing the size of the hidden layers. For both architectures, we evaluated smaller networks with approximately 60K and 80K parameters, along with the networks used in our main studies, which had roughly 100K parameters. For the three datasets used in our study, we evaluated the test error of the neural networks of various sizes, trained using the protocol described in Section 2, including averaging over ten runs.

Figure 15 plots the average test errors, as a function of the size of the model. In all cases, the test error does not improve much as the size of the model increases from $\approx 60K$ to $\approx 100K$.



(a) Plots for MNIST 3-vs-8 and 5-vs-6.

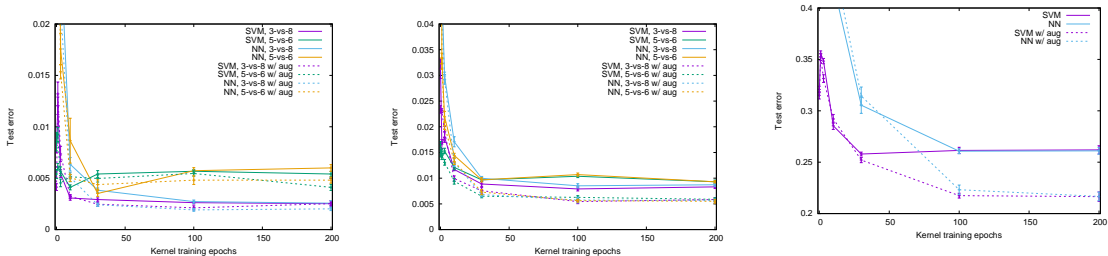


(b) Plots for CIFAR10 cats-vs-dogs

Figure 15: A plot of the average test error of neural networks as a function of the parameters in the network, for different architectures and numbers of epochs of training.

B Sanity check: augmentations improve accuracy

Figure 16 reproduces the well-known fact that data augmentations improve the test accuracy of learned models.



(a) A plot of the test errors of the SVM model, and the NN model that trained the kernel for the SVM model, with and without data augmentation, on the VGG-like models.

(b) A plot of the test errors of the SVM model, and the NN model that trained the kernel for the SVM model, with and without data augmentation, on the fully connected model.

(c) A plot of the test errors of the SVM model, and the NN model that trained the kernel for the SVM model, with and without data augmentation, for the VGG-like model trained on cats-vs-dogs.

Figure 16: Test error of models with and without data augmentation.